

Separable representation of phenomenological optical potentials of Woods-Saxon type

L. Hlophe,^{1,*} Ch. Elster,^{1,†} R. C. Johnson,² N. J. Upadhyay,³ F. M. Nunes,³ G. Arbanas,⁴ V. Eremenko,^{1,6}
J. E. Escher,⁵ and I. J. Thompson⁵
(TORUS Collaboration)

¹*Institute of Nuclear and Particle Physics, and Department of Physics and Astronomy, Ohio University, Athens, Ohio 45701, USA*

²*Department of Physics, University of Surrey, Guildford GU2 7XH, United Kingdom*

³*National Superconducting Cyclotron Laboratory and Department of Physics and Astronomy, Michigan State University, East Lansing, Michigan 48824, USA*

⁴*Nuclear Science and Technology Division, Oak Ridge National Laboratory, Oak Ridge, Tennessee 37831, USA*

⁵*Lawrence Livermore National Laboratory, L-414, Livermore, California 94551, USA*

⁶*D.V. Skobeltsyn Institute of Nuclear Physics, M.V. Lomonosov Moscow State University, Moscow 119991, Russia*

(Received 1 November 2013; published 11 December 2013)

Background: One important ingredient for many applications of nuclear physics to astrophysics, nuclear energy, and stockpile stewardship are the cross sections for reactions of neutrons with rare isotopes. Since direct measurements are often not feasible, indirect methods, e.g., (d, p) reactions, should be used. Those (d, p) reactions may be viewed as three-body reactions and described with Faddeev techniques.

Purpose: Faddeev equations in momentum space have a long tradition of utilizing separable interactions in order to arrive at sets of coupled integral equations in one variable. While there exist several separable representations for the nucleon-nucleon interaction, the optical potential between a neutron (proton) and a nucleus is not readily available in separable form. The purpose of this paper is to introduce a separable representation for complex phenomenological optical potentials of Woods-Saxon type.

Results: Starting from a global optical potential, a separable representation thereof is introduced based on the Ernst-Shakin-Thaler (EST) scheme. This scheme is generalized to non-Hermitian potentials. Applications to $n + {}^{48}\text{Ca}$, $n + {}^{132}\text{Sn}$, and $n + {}^{208}\text{Pb}$ are investigated for energies from 0 to 50 MeV and the quality of the representation is examined.

Conclusions: We find a good description of the on-shell t matrix for all systems with rank up to 5. The required rank depends inversely on the angular momentum. The resulting separable interaction exhibits a different off-shell behavior compared to the original potential, reducing the high-momentum contributions.

DOI: [10.1103/PhysRevC.88.064608](https://doi.org/10.1103/PhysRevC.88.064608)

PACS number(s): 24.10.Ht, 25.10.+s, 25.40.Dn

I. INTRODUCTION

A variety of applications of nuclear physics require an understanding of neutron capture on unstable nuclei. Due to the short lifetimes involved, direct measurements are currently not possible, and thus indirect methods using (d, p) reactions have been proposed (see, e.g., Refs. [1–3]). Single-neutron-transfer (d, p) reactions have also been the preferred tool to study shell evolution in nuclear structure (see, e.g., Refs. [4,5]). In all these cases, a reliable reaction theory is a critical ingredient.

Scattering and reaction processes involving deuterons either as projectile or as target are perhaps the most natural three-body problem in the realm of nuclear reactions. The binding energy of the deuteron is so small that its root-mean-square radius is significantly larger than the range of the force. That means, when a deuteron interacts with a compact nucleus, one may expect that it will behave like a three-body system consisting of a proton p , a neutron n , and a nucleus A . The obvious three-body reactions are elastic scattering, rearrangement, and breakup processes. In order to describe those processes on the same footing, deuteron-nucleus scattering

should be treated as a three-body problem with a three-body Hamiltonian governing the dynamics. This three-body Hamiltonian contains the well-understood nucleon-nucleon (NN) interaction as well as the effective interactions between the nucleons and the target (nA and pA). It is common for these nucleons-nucleus interactions to take phenomenological optical potentials which fit a large body of elastic scattering data [6–9].

The application of momentum-space Faddeev techniques to nuclear reactions has been pioneered in Ref. [10] and successfully applied to (d, p) reactions for light nuclei [11]. However, when extending these calculations to heavier nuclei [12,13], it becomes apparent that techniques employed for incorporating the Coulomb interaction in Faddeev-type calculations of reactions with light nuclei cannot readily be extended to the heaviest nuclei. Therefore, a new method for treating (d, p) reactions with the exact inclusion of the Coulomb force as well as target excitation was formulated in Ref. [14]. This new approach relies on a separable representation of the interparticle forces.

Separable representations of the forces between constituents forming the subsystems in a Faddeev approach have a long tradition in few-body physics. There is a large body of work on separable representations of NN interactions (see, e.g., Refs. [15–19]) or meson-nucleon interactions [20,21].

*lh421709@ohio.edu

†elster@ohio.edu

In the context of describing light nuclei such as ${}^6\text{He}$ [22] and ${}^6\text{Li}$ [23] in a three-body approach, separable interactions have been successfully used. A separable nucleon- ${}^{12}\text{C}$ optical potential was proposed in Ref. [24]; it consists of a rank-1 Yamaguchi-type form factor fitted to the positive energies and a similar term describing the bound states in the nucleon- ${}^{12}\text{C}$ configuration. However, we are not aware of any systematic work along this line for heavy nuclei, for which excellent phenomenological descriptions exist in terms of Woods-Saxon functions [6–9]. For applications to (d, p) reactions there is a need for a procedure for deriving a separable representation that is sufficiently general for a variety of nucleon-nucleus optical potentials, as well as over a wide range of nuclei and energies, so that one can take advantage of the already existing extensive work on phenomenological optical potentials.

The separable representation of two-body interactions suggested by Ernst-Shakin-Thaler [25] (EST) seems well suited for achieving this goal. We note that this EST approach has been successfully employed to represent NN potentials [15,16]. However, in the EST representation as derived in Ref. [25], though energy dependence of the potentials is allowed [26,27], it is assumed that they are Hermitian. Therefore, the EST approach needs to be generalized in order to be applicable for optical potentials which are complex.

In Sec. II we present the generalization of the EST approach to non-Hermitian potentials needed so that the potential as well as the transition matrix fulfills the reciprocity theorem. First, we explicitly show for a rank-1 separable potential the required redefinition of the separable ansatz of Ref. [25], and then we generalize to separable potentials of arbitrary rank. Since all our calculations are carried out in momentum space, we sketch the explicit procedure to obtain separable transition matrices. This procedure follows closely the one laid out in Ref. [25], and we will refer to it as the EST scheme.

In Sec. III A we present the results for the separable representations of optical potentials for ${}^{48}\text{Ca}$, ${}^{132}\text{Sn}$, and ${}^{208}\text{Pb}$ based on the CH89 [6] phenomenological optical potential. Note that the definition of the optical potential in coordinate space and details on the Fourier transform and partial wave decomposition are presented in the Appendix. In Sec. III B, we investigate the off-shell behavior of the separable representations and compare it to the original potential. Finally, we summarize our findings in Sec. IV.

II. FORMAL CONSIDERATIONS

A scheme for constructing separable potentials from the solution of a Lippmann-Schwinger (LS) equation with arbitrary Hermitian potentials was suggested by Ernst, Shakin, and Thaler [25]. This separable potential is designed to represent the scattering matrix (or equivalently the scattering phase shifts) over a chosen energy range with the same quality as the original potential. Furthermore, this EST scheme provides a well-defined prescription for increasing the accuracy of the representation by increasing the rank of the separable potential.

The basic idea of the EST scheme for constructing a separable representation of the two-body transition amplitude is that one selects a fixed number of energy points in the energy

interval in which the separable potential shall represent the scattering matrix. At these chosen points, the on-shell as well as half-shell t matrices of the original potential are identical to those obtained with the separable potential. The corresponding half-shell t matrices at these points then serve as form factors of the separable representation. The number of these fixed points gives the rank of the separable potential.

The EST [25,26] scheme has been successfully applied to construct separable representations of several NN potentials [15,16] defined below the pion production threshold, i.e., real potentials. Potentials intended to describe the scattering of neutrons or protons from nuclei are in general complex as a result of reactions channels not explicitly taken into account. In the following we show that the formulation given in Ref. [25] is not suitable for complex potentials, since it is not compatible with the reciprocity theorem. We illustrate how the requirement of time-reversal invariance leads to a modification of the definition of the separable potential.

A. Separable complex potentials of rank 1 and time reversal

For applications to the theory of nuclear reactions it is convenient to arrange that all potential operators U satisfy

$$\mathcal{K}U\mathcal{K}^{-1} = U^\dagger, \quad (1)$$

where \mathcal{K} is the time-reversal operator appropriate to the system. This condition guarantees that the S matrix corresponding to U is symmetric and that reaction amplitudes constructed from these potentials satisfy convenient reciprocity relations.

When U is a central potential in the space of a spinless particle, \mathcal{K} can be chosen to be the antilinear complex conjugation operator \mathcal{K}_0 , which in the coordinate-space basis $|\mathbf{r}\rangle$ is defined by

$$\mathcal{K}_0 \alpha |\mathbf{r}\rangle = \alpha^* (\mathcal{K}_0 |\mathbf{r}\rangle) = \alpha^* |\mathbf{r}\rangle, \quad (2)$$

and from which we deduce $\mathcal{K}_0 |\mathbf{p}\rangle = |-\mathbf{p}\rangle$. Note that for this particular \mathcal{K} we have $(\mathcal{K}_0)^{-1} = \mathcal{K}_0$.

We first consider a Hermitian interaction v acting in a partial wave with angular momentum l . It was shown in Ref. [25] that a rank-1 separable potential leading to a scattering wave function that is identical to that of potential V (defined via a Hamiltonian $H = H_0 + V$) at a specific energy E_{k_E} (support point) is given as

$$\mathbf{V}(E_{k_E}) = \frac{v |f_{l,k_E}\rangle \langle f_{l,k_E}| v}{\langle f_{l,k_E}| v |f_{l,k_E}\rangle} \equiv v |f_{l,k_E}\rangle \hat{\lambda} \langle f_{l,k_E}| v. \quad (3)$$

Here $|f_{l,k_E}\rangle$ is the regular radial scattering wave function, which is unique within an overall constant, for v at energy E_{k_E} , $v |f_{l,k_E}\rangle$ is the form factor, and $(\hat{\lambda})^{-1} = \langle f_{l,k_E}| v |f_{l,k_E}\rangle$ is the strength parameter.

For a Hermitian v the radial function f_{l,k_E} can be taken to be real in both coordinate and momentum space and the strength parameter $\hat{\lambda}$ is real. As a result, the nonlocal potential \mathbf{V} of Eq. (3) is a Hermitian symmetric matrix in both momentum and coordinate space and satisfies $\mathcal{K}_0 \mathbf{V} \mathcal{K}_0 = \mathbf{V}^\dagger$.

If however v is a complex potential, or more generally a non-Hermitian operator u , the radial functions f_{l,k_E} are no longer real and if v is simply replaced by u in Eq. (3) the

resulting rank-1 nonlocal potential U will neither be Hermitian nor satisfy $\mathcal{K}_0 U \mathcal{K}_0 = U^\dagger$.

To remedy this situation for a non-Hermitian potential u we replace the definition of Eq. (3) by

$$\mathbf{U}(E_{k_E}) \equiv \frac{u |f_{l,k_E}\rangle \langle f_{l,k_E}^*| u}{\langle f_{l,k_E}^*| u |f_{l,k_E}\rangle} \equiv u |f_{l,k_E}\rangle \hat{\lambda} \langle f_{l,k_E}^*| u, \quad (4)$$

where now the strength parameter is defined by $(\hat{\lambda})^{-1} = \langle f_{l,k_E}^*| u |f_{l,k_E}\rangle$.

Here $f_{l,k_E}(r)$ is the unique regular radial wave function corresponding to u and $f_{l,k_E}^*(r)$ is the unique regular radial wave function corresponding to u^* . By a suitable choice of arbitrary normalization constants we can arrange that $f_{l,k_E}^*(r)$ is simply the complex conjugate of f_{l,k_E} and hence $\mathcal{K}_0 |f_{l,k_E}\rangle = |f_{l,k_E}^*\rangle$.

If u satisfies $\mathcal{K}_0 u \mathcal{K}_0 = u^\dagger$ the definition of Eq. (4) gives a symmetric complex potential matrix that satisfies

$$\begin{aligned} \mathcal{K}_0 \mathbf{U}(E_{k_E}) \mathcal{K}_0 &= (\mathcal{K}_0 u |f_{l,k_E}\rangle) (\hat{\lambda})^* (\langle f_{l,k_E}^*| u \mathcal{K}_0) \\ &= u^\dagger |f_{l,k_E}^*\rangle (\hat{\lambda})^* \langle f_{l,k_E}^*| u^\dagger = U^\dagger, \end{aligned} \quad (5)$$

where the round brackets mean that \mathcal{K}_0 here acts only on the quantities within the brackets.

For a general energy E and arbitrary potential \mathcal{V} we define an operator $t(E)$ as the solution of

$$t(E) = \mathcal{V} + \mathcal{V} g_0(E) t(E). \quad (6)$$

$$\begin{aligned} \tau(E)^{-1} &= t(k_E, k_E, E_{k_E}) + 2\mu \left[\mathcal{P} \int dp p^2 \frac{t(p, k_E, E_{k_E}) t(p, k_E, E_{k_E})}{k_E^2 - p^2} - \mathcal{P} \int dp p^2 \frac{t(p, k_E, E_{k_E}) t(p, k_E, E_{k_E})}{k_0^2 - p^2} \right] \\ &\quad + i\pi\mu [k_0 t(k_0, k_E, E_{k_E}) t(k_0, k_E, E_{k_E}) - k_E t(k_E, k_E, E_{k_E}) t(k_E, k_E, E_{k_E})]. \end{aligned} \quad (11)$$

Here the half-shell t matrices $t(p, k_E, E_{k_E})$ are the momentum-space solutions of a standard LS equation at the scattering energy E_{k_E} .

Thus, the rank-1 separable potential as given in Eq. (4) leads to the desired rank-1 separable t matrix, which fulfills the reciprocity theorem.

B. Separable complex potentials of arbitrary rank

It remains to generalize the above formulation of a rank-1 separable complex potential to one of arbitrary rank. In analogy to the procedure followed in Ref. [25] we define a complex separable potential of arbitrary rank in a given partial wave as

$$\mathbf{U} = \sum_{i,j} u |f_{l,k_{E_i}}\rangle \langle f_{l,k_{E_i}}| M |f_{l,k_{E_j}}^*\rangle \langle f_{l,k_{E_j}}^*| u. \quad (12)$$

Here $f_{l,k_{E_i}}$ is the unique regular radial wave function corresponding to the complex potential u and asymptotic energy E_i , and $f_{l,k_{E_j}}^*$ is the unique regular radial wave function corresponding to u^* . Note that u may also be energy dependent.

For the potential given by Eq. (4) we then obtain a rank-1 separable t matrix $t(E)$ in a given partial wave with matrix elements

$$\langle p'| t(E) |p\rangle = \frac{\langle p'| u |f_{l,k_E}\rangle \langle f_{l,k_E}^*| u |p\rangle}{\langle f_{l,k_E}^*| u - u g_0(E) u |f_{l,k_E}\rangle}. \quad (7)$$

By introducing $t(p', k_E, E_{k_E}) = \langle f_{l,k_E}^*| u |p'\rangle$ and $t(p, k_E, E_{k_E}) = \langle p| u |f_{l,k_E}\rangle$, the partial wave t matrix element $\langle p'| t(E) |p\rangle$ can be written as

$$\begin{aligned} \langle p'| t(E) |p\rangle &= \frac{t(p', k_E, E_{k_E}) t(p, k_E, E_{k_E})}{\langle f_{l,k_E}^*| u (1 - g_0(E) u) |f_{l,k_E}\rangle} \\ &\equiv t(p', k_E, E) \tau(E) t(p, k_E, E), \end{aligned} \quad (8)$$

where

$$\tau^{-1}(E) = \langle f_{l,k_E}^*| u (1 - g_0(E) u) |f_{l,k_E}\rangle. \quad (9)$$

The scattering wave function $|f_{l,k_E}\rangle$ satisfies $|f_{l,k_E}\rangle = |k_E\rangle + g_0(E_{k_E}) u |f_{l,k_E}\rangle$. Using this we find $[\tau(E_{k_E})]^{-1} = \langle k_E| u |f_{l,k_E}\rangle = t(k_E, k_E, E_{k_E})$, and hence

$$\langle p'| t(E_{k_E}) |p\rangle = \frac{t(p', k_E, E_{k_E}) t(p, k_E, E_{k_E})}{t(k_E, k_E, E_{k_E})}, \quad (10)$$

where angular momentum indices are omitted.

On the energy shell, i.e., for $p \rightarrow k_E$ and $p' \rightarrow k_E$, the separable t matrix of Eq. (10) agrees with the t matrix evaluated with the original potential u , as it should. For any general $E = k_0^2/2\mu$ the function $\tau(E)$ of Eq. (8) is explicitly calculated as

The matrix M is defined and constrained by

$$\begin{aligned} \delta_{ik} &= \sum_j \langle f_{l,k_{E_i}} | M |f_{l,k_{E_j}}^*\rangle \langle f_{l,k_{E_j}}^* | u |f_{l,k_{E_k}}\rangle \\ &= \sum_j \langle f_{l,k_{E_i}}^* | u |f_{l,k_{E_j}}\rangle \langle f_{l,k_{E_j}} | M |f_{l,k_{E_k}}^*\rangle. \end{aligned} \quad (13)$$

The corresponding separable partial wave t matrix must be of the form

$$t(E) = \sum_{i,j} u |f_{l,k_{E_i}}\rangle \tau_{ij}(E) \langle f_{l,k_{E_j}}^*| u, \quad (14)$$

where angular momentum indices are omitted for simplicity of notation. The coefficient matrix $\tau_{ij}(E)$ is constrained by

$$\sum_i \langle f_{l,k_{E_i}}^* | u - u g_0(E) u |f_{l,k_{E_i}}\rangle \tau_{ij}(E) = \delta_{nj}, \quad (15)$$

and

$$\sum_j \tau_{ij}(E) \langle f_{l,k_{E_j}}^* | u - u g_0(E) u |f_{l,k_{E_k}}\rangle = \delta_{ik}. \quad (16)$$

For $i = j = 1$ we recover the expressions for the rank-1 potential of the previous section.

For the explicit calculation of the matrix $\tau_{ij}(E)$, we define a matrix

$$R_{ij}(E) \equiv \langle f_{l,k_{E_i}}^* | u - u g_0(E) u | f_{l,k_{E_j}} \rangle, \quad (17)$$

so that the condition of Eq. (16) reads

$$\sum_j \tau_{ij}(E) R_{jk}(E) = \delta_{ik}, \quad (18)$$

from which follows

$$\tau_{ij}(E) = [R(E)]_{ij}^{-1}. \quad (19)$$

By using again that $t(p', k_{E_i}, E_i) = \langle f_{l,k_{E_i}}^* | u | p' \rangle$ and $t(p, k_{E_i}, E_i) = \langle p | u | f_{l,k_{E_i}} \rangle$, the matrix elements R_{ij} are calculated in momentum space. With $E = k_0^2/2\mu$, the diagonal matrix elements are given as

$$\begin{aligned} R_{ii}(E) &= \langle f_{l,k_{E_i}}^* | u - u g_0(E) u | f_{l,k_{E_i}} \rangle \\ &= t(k_{E_i}, k_{E_i}; E_i) + 2\mu \\ &\quad \times \mathcal{P} \int dp p^2 \frac{t(p, k_{E_i}; E_i) t(p, k_{E_i}; E_i)}{k_{E_i}^2 - p^2} \\ &\quad - i\pi k_{E_i} t(k_{E_i}, k_{E_i}; E_i) t(k_{E_i}, k_{E_i}; E_i) \\ &\quad - 2\mu \mathcal{P} \int dp p^2 \frac{t(p, k_{E_i}; E_i) t(p, k_{E_i}; E_i)}{k_0^2 - p^2} \\ &\quad + i\pi k_0 t(k_0, k_{E_i}; E_i) t(k_0, k_{E_i}; E_i). \end{aligned} \quad (20)$$

The half-shell t matrices $t(p, k_{E_i}; E_i)$ are the momentum-space solutions of a standard LS equation at the support points E_i . At these energies E_i , the on-shell t -matrix elements calculated from the separable potential agree with those calculated from the original complex potential u .

The off-diagonal elements of the matrix $R_{ij}(E)$ are given by

$$\begin{aligned} R_{ij}(E) &= \langle f_{l,k_{E_i}}^* | u - u g_0(E) u | f_{l,k_{E_j}} \rangle \\ &= t(k_{E_j}, k_{E_i}; E_i) + 2\mu \\ &\quad \times \mathcal{P} \int dp p^2 \frac{t(p, k_{E_i}; E_i) t(p, k_{E_j}; E_j)}{k_{E_j}^2 - p^2} \\ &\quad - i\pi \mu k_{E_j} t(k_{E_j}, k_{E_i}; E_i) t(k_{E_j}, k_{E_j}; E_j) \\ &\quad - 2\mu \mathcal{P} \int dp p^2 \frac{t(p, k_{E_i}; E_i) t(p, k_{E_j}; E_j)}{k_0^2 - p^2} \\ &\quad + i\pi \mu k_0 t(k_0, k_{E_i}; E_i) t(k_0, k_{E_j}; E_j). \end{aligned} \quad (21)$$

The matrix elements $R_{ij}(E)$, where i, j determine the rank of the separable representation, are calculated at a fixed number of energy support points E_i . The elements $\tau_{ij}(E)$ are then obtained by solving a system of linear equations $\mathbf{R}\boldsymbol{\tau} = \mathbf{1}$. For this to be successful, the inverse of $R_{ij}(E)$ must exist. For calculating the form factors, the half-shell t matrices at the support points E_i are calculated by solving a LS equation with the momentum-space Woods-Saxon potential derived in the Appendix. For calculating the matrix elements $R_{ij}(E)$ we use the cubic Hermite spline interpolation of Ref. [28] to obtain

the values at the required momenta. Since spline functions are by design linearly independent, the representation of the half-shell t matrices in this basis guarantees that the matrix $R_{ij}(E)$ is always invertible.

In order to calculate the momentum-space partial wave separable potential, one needs to evaluate Eq. (12),

$$\langle k' | \mathbf{U} | k \rangle = \sum_{i,j} \langle k' | u | f_{l,k_{E_i}} \rangle \langle f_{l,k_{E_i}} | M | f_{l,k_{E_j}}^* \rangle \langle f_{l,k_{E_j}}^* | u | k \rangle, \quad (22)$$

together with the constraint of Eq. (13). The matrix elements

$$W_{ij} \equiv \langle f_{l,k_{E_i}}^* | u | f_{l,k_{E_j}} \rangle \quad (23)$$

are already part of the computation of the matrix elements $R_{ij}(E)$ from Eqs. (20) and (21). The coefficient matrix $M_{ij} \equiv \langle f_{l,k_{E_i}}^* | M | f_{l,k_{E_j}} \rangle$ is then obtained as the inverse of W_{ij} .

III. RESULTS

A. On-shell behavior of the optical potential and its separable representation

To demonstrate the construction of a separable representation of a complex potential we apply the method to $n + {}^{48}\text{Ca}$, $n + {}^{132}\text{Sn}$, and $n + {}^{208}\text{Pb}$ and use as a starting point the Chapel Hill phenomenological global optical potential CH89 [6]. CH89 has been widely used in the literature in the last decades and also in recent studies of (d, p) reactions [4,5].

By using Woods-Saxon functions as parametrized forms, these phenomenological global optical potentials are most naturally given in coordinate space. For convenience, in these global parametrizations one must assume local form factors of the interaction but must introduce an explicit energy dependence in the strengths.

In order to construct a separable momentum-space representation of CH89 using the scheme outlined in the previous section, we first must derive a momentum-space representation of the CH89 optical potential. The explicit evaluation of the Fourier transform of the CH89 potential, including the final expressions we have implemented, is given in the Appendix, but there are a few essential points worth highlighting. The Fourier transform of the coordinate-space Woods-Saxon function into momentum space can be written as a series expansion. Fortunately, we found, by the explicit calculation of the leading terms of this expansion, that only the first two terms are necessary to obtain a converged result. These expressions were used as input to a momentum-space LS equation, and the resulting phase shifts were compared to those computed with the coordinate-space CH89 potential using FRESKO [29]. Agreement was found for three significant figures.

A separable t matrix constructed within the scheme outlined in Sec. II from a t matrix calculated as solution of an LS equation with a given potential is exact on-shell as well as half-shell at fixed support points E_i . For any other energy $E \neq E_i$ it is then calculated by using Eq. (14).

For studying the quality of the separable representation it is convenient to look at the partial wave S matrix, given as

$$S_l(E) = 1 + 2i \hat{\tau}_l(E), \quad (24)$$

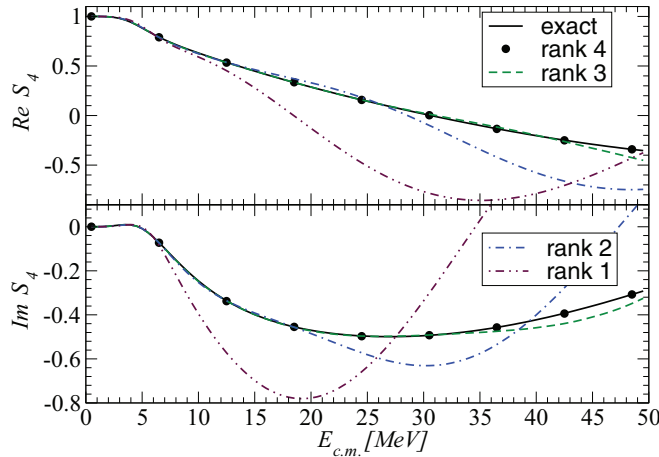


FIG. 1. (Color online) The $l = 4$ ($j = 9/2$) partial wave S matrix for the $n + {}^{48}\text{Ca}$ system obtained from the CH89 [6] phenomenological optical potential as a function of the c.m. energy. The exactly calculated S matrix is given by the solid line. Separable representations of rank 1 (support point at 6 MeV), rank 2 (support points at 6 and 12.5 MeV), and rank 3 (support points at 6, 15, and 25 MeV) are shown by the dash-double-dotted, dash-dotted, and dashed lines, respectively. The rank-4 representation (support points at 6, 15, 36, and 47 MeV) coincides with the exact calculation and is indicated by the solid dots.

where E represents the center-of-mass (c.m.) energy, $E \equiv E_{c.m.}$. The dimensionless amplitude $\hat{t}_l(E)$ is given by

$$\hat{t}_l(E) = -\pi \mu k_0 t_l(k_0, k_0; E). \quad (25)$$

The on-shell momentum k_0 is defined via $E_{c.m.} = k_0^2/2\mu$, and μ is the reduced mass of the system under consideration. The partial wave t matrix, $t_l(k_0, k_0)$, is either calculated directly from the CH89 potential or obtained via our general scheme to construct a separable representation thereof.

First we study in detail the scheme for constructing a separable representation of the $n + {}^{48}\text{Ca}$ system for c.m. energies from 0 to 50 MeV. Our goal is to arrive at an excellent separable representation of the partial wave S matrix starting from the local CH89 potential. For practical applications in, e.g., three-body type calculations, it is desirable to achieve this with as low a rank as possible. As a representative case, we show the $l = 4$, $j = 9/2$ partial wave S matrix in Fig. 1. The S matrix obtained from the solution of the LS equation with the original CH89 optical potential (solid line) shows a relatively mild variation with energy in the energy regime under consideration. If one is only interested in describing the very low energies, i.e., $E_{c.m.} \leq 10$ MeV, a rank-1 separable potential with a support point at 6 MeV is barely sufficient (dash-double-dotted line), while a rank-2 representation with support points at 6 and 12.5 MeV can already capture the range between 0 and 20 MeV relatively well. A rank-3 representation with support points at 5, 15, and 25 MeV captures the S matrix up to roughly 35 MeV. However, for a high-quality separable representation of at least four significant figures of the CH89 result a rank-4 representation with support points at 6, 15, 36, and 47 MeV is needed in this partial wave. The figure also shows that more support points are needed in the region where

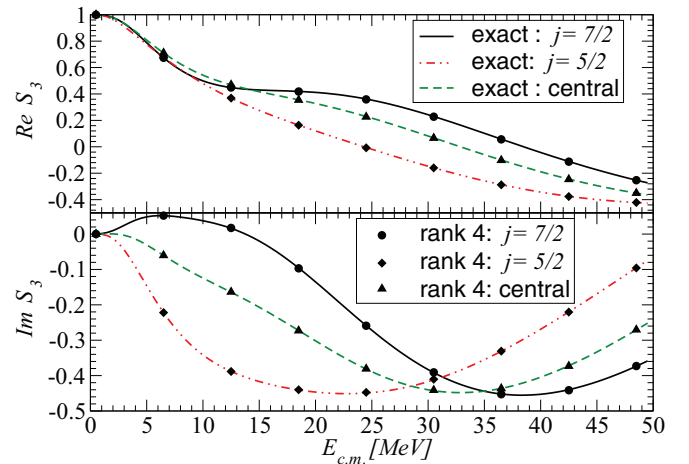


FIG. 2. (Color online) The $l = 3$ partial wave S matrix for the $n + {}^{48}\text{Ca}$ system obtained from the CH89 [6] phenomenological optical potential as a function of the c.m. energy. The exactly calculated partial wave S matrices for $j = 7/2$, $j = 5/2$, and the central part of the optical potential alone are given by the solid, dash-double-dotted, and dashed lines, respectively. The results for the corresponding rank-4 separable representations (support points at 6, 15, 36, and 47 MeV) are overlaid and indicated by the solid symbols as indicated in the figure.

the S matrix shows structure, and less points are necessary for the smooth region.

The next question for a practical implementation of the EST scheme is whether the optimum support points when including both central and spin-orbit interactions differ from the results when including the central interaction only. Usually the central part of an optical potential is larger than the spin part. Thus one may expect it to be sufficient to find EST support points for the S matrix computed using only the central part of the optical potential, and then use the same points for deriving the separable representation of the $l \pm 1/2$ partial wave S matrices. This is indeed the case, as is demonstrated for the $l = 3$ partial wave S matrix for the $n + {}^{48}\text{Ca}$ system in Fig. 2. The dashed line shows the S matrix calculated from the central part of the CH89 optical potential, while the solid and dash-double-dotted lines represent the $l + 1/2$ and the $l - 1/2$ partial wave S matrices, respectively. Our results show that it is indeed sufficient to determine the EST support points for the S matrix computed from the central part of the optical potential. Thus, once the support points are determined from a calculation including the central part, one only needs to replace the corresponding form factors, i.e., the half-shell t matrices, at the support points with the ones containing the spin-orbit contribution to obtain the separable representation of the $l \pm 1/2$ partial wave S matrices with unchanged accuracy.

For the $n + {}^{48}\text{Ca}$ system we find that for the lower partial waves a rank-4 separable representation is sufficient for energies up to $E_{c.m.} = 50$ MeV. Let us now consider what happens as we increase the angular momentum. Reaction calculations in the energy range 0–50 MeV often require partial waves up to $l = 20$, but due to the centrifugal barrier with increasing angular momentum the t matrix remains close to zero even at higher scattering energy. Therefore, one

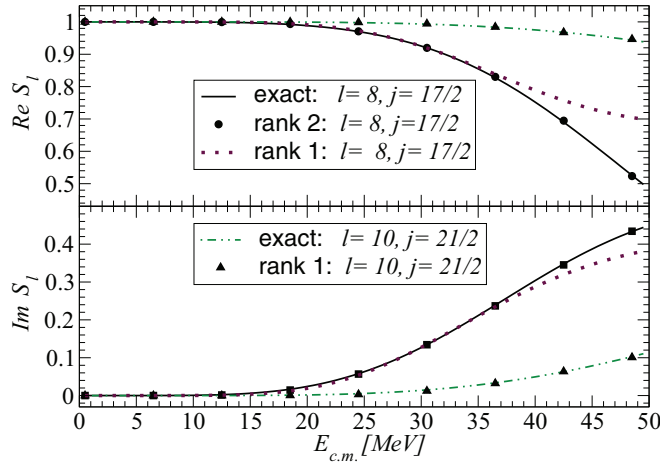


FIG. 3. (Color online) The $l = 8, j = 17/2$ (solid line) and $l = 10, j = 21/2$ (dash-double-dotted line) partial wave S matrices for the $n + {}^{48}\text{Ca}$ system calculated from the CH89 [6] phenomenological optical potential as functions of the c.m. energy. The rank-1 (support point at 29 MeV) and rank-2 (support points at 29 and 47 MeV) representations for the $l = 8$ partial wave S matrix are given by the dotted line and the filled circles, respectively. The rank-1 (support point at 40 MeV) representation for the $l = 10$ partial wave S matrix is indicated by the filled triangles.

may expect, for the same accuracy, a lower rank separable representation to suffice for representing higher partial waves. This is indeed the case as demonstrated in Fig. 3. Here we show the $l = 8, j = 17/2$ and $l = 10, j = 21/2$ partial wave S matrices and their corresponding separable representation. We find that for $l = 10$ a rank-1 representation is sufficient up to $E_{c.m.} = 50$ MeV, whereas the $l = 8$ partial wave S matrix still requires a rank-2 representation. For the energy regime under consideration, we determined the angular momentum intervals in which separable representations of specific ranks represent the original partial wave S matrices within four significant figures. Those angular momentum groups and their corresponding support points are listed in Table I.

TABLE I. The EST support points at c.m. energies E_{k_i} used for constructing the separable representation of the partial wave S matrix of the $n + {}^{48}\text{Ca}$ and $n + {}^{208}\text{Pb}$ systems. The support points in the last row for the $n + {}^{208}\text{Pb}$ system given in boldface indicate the universal set of support points, which can be used to construct a representation for all nuclei given by the CH89 [6] phenomenological optical potential.

System	Partial wave(s)	Rank	EST support point(s) (MeV)
$n + {}^{48}\text{Ca}$	$l \geq 10$	1	40
	$l \geq 8$	2	29, 47
	$l \geq 6$	3	16, 36, 47
	$l \geq 0$	4	6, 15, 36, 47
$n + {}^{132}\text{Sn}$	$l \geq 16$	1	40
	$l \geq 13$	2	35, 48
and	$l \geq 11$	3	24, 39, 48
$n + {}^{208}\text{Pb}$	$l \geq 6$	4	11, 21, 36, 45
	$l \geq 0$	5	5, 11, 21, 36, 47

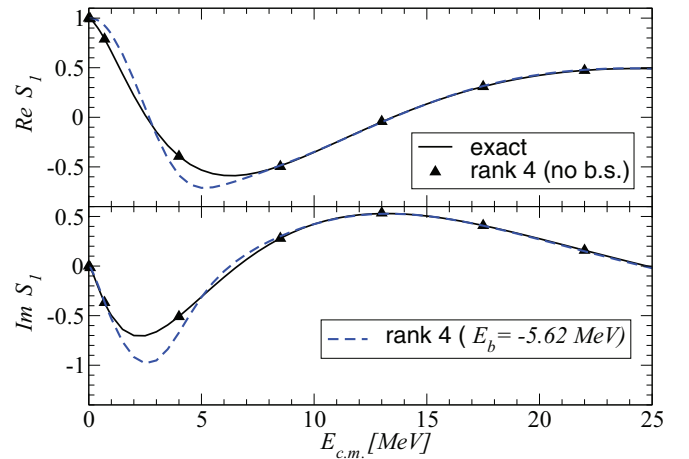


FIG. 4. (Color online) The $l = 1 (j = 3/2)$ partial wave S matrix for the $n + {}^{48}\text{Ca}$ system obtained from the CH89 [6] phenomenological optical potential as a function of the c.m. energy. The exactly calculated S matrix is given by the solid line. A separable representation of rank 4 (support points at 6, 15, 36, and 47 MeV) is indicated by the filled triangles. For the dashed line the lowest support point at 6 MeV is replaced by a point at the bound state $E_b = -5.62$ MeV.

Support points need not be at positive energies; therefore a bound state may be included and this is exactly the situation in the so-called unitary pole approximation [30]. Given our original purpose [namely, a Faddeev description of (d, p) reactions], a good description of the final bound state will be necessary. To understand the effect of including a bound state in the separable representation, we consider the $l = 1, j = 3/2$ partial wave S matrix of the $n + {}^{48}\text{Ca}$ system, which would correspond to the partial wave of the valence neutron in the ground state of ${}^{49}\text{Ca}$. When extrapolating the CH89 parametrization to $E_{c.m.} < 0$, we set the imaginary part to zero and directly extrapolate the real part with no further fitting, just for the sake of illustrating the method here. With such an approach, we find two bound states with energies $E_b = -28.8$ MeV and $E_b = -5.62$ MeV. We now move the support point at 6 MeV to $E_b = -5.62$ MeV, which would be the valence orbital in this system. The results are shown in Fig. 4. The solid line shows the exact calculation, the solid triangles are its separable rank-4 representation. The so-obtained rank-4 separable representation is given by the dashed line in Fig. 4. Though the bound state is relatively close to threshold, the deviation from the original representation and the exact S matrix is quite large in the region between 1 and 7 MeV, indicating that the low-energy support point is needed for capturing the structure of this partial wave S matrix at low energies.

From this study we learn that though it is very easy to add bound states to the separable representation of a specific partial wave S matrix, such a bound state, even if shallow, does not necessarily replace a low-energy support point. For an application to (d, p) reactions, one should add a bound state corresponding to the final state populated through the reaction, thus increasing the rank by one.

Up to now we studied the separable representations in detail for the $n + {}^{48}\text{Ca}$ system. Next, we turn to a heavy nuclei and

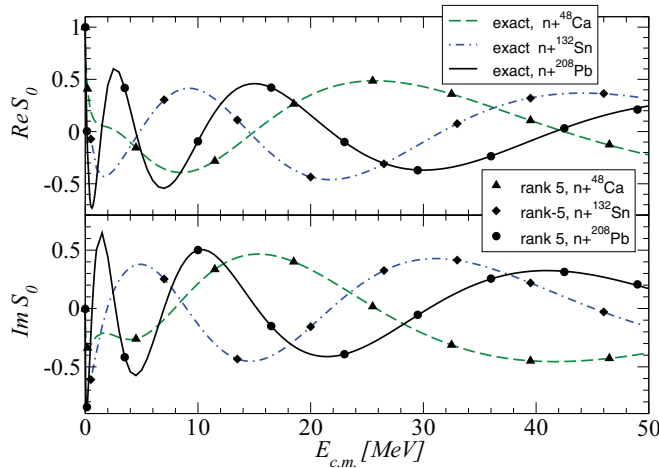


FIG. 5. (Color online) The $l = 0$ partial wave S matrices for the $n + {}^{48}\text{Ca}$ system (dashed line), the $n + {}^{132}\text{Sn}$ system (dash-dotted line), and the $n + {}^{208}\text{Pb}$ system (solid line) calculated exactly from the CH89 [6] phenomenological optical potential as functions of the c.m. energy. A rank-5 representation (support points at 5, 11, 21, 36, and 47 MeV) for both systems is overlaid and indicated by the filled circles ($n + {}^{208}\text{Pb}$), the filled diamonds ($n + {}^{132}\text{Sn}$), and the filled triangles ($n + {}^{48}\text{Ca}$).

repeat the study for the $n + {}^{132}\text{Sn}$ and $n + {}^{208}\text{Pb}$ systems. In these cases, the partial wave S matrices have more structure, and thus they require more support points for an accurate representation. For different partial waves, we again find that we have groups of angular momenta for which a specific rank is required to represent the partial wave S matrix to an accuracy of at least four significant figures. These groups and the energies of the corresponding support points are summarized in Table I. First we note that a separable representation of rank 5 is sufficient for the low-angular-momentum states. Similar to the $n + {}^{48}\text{Ca}$ system, the higher angular momentum states require successively fewer support points. However, in order for a rank-1 representation to be accurate in the energy regime under consideration, one must go up to $l = 16$.

Considering the number of support points needed for medium-mass ($n + {}^{48}\text{Ca}$) and heavy ($n + {}^{132}\text{Sn}$ and $n + {}^{208}\text{Pb}$) systems, we find it encouraging that a very good description of the heavy systems can be achieved by increasing the rank of the representation by only one, relative to the medium-mass case.

If we are interested in a “universal” separable representation for partial wave t matrices obtained from the CH89 optical potential, we can use the support points obtained for the $n + {}^{208}\text{Pb}$ system, apply them to all other systems, and obtain a high-quality separable representation. This is shown in Fig. 5 for the $l = 0$ partial wave S matrix for the $n + {}^{48}\text{Ca}$, $n + {}^{132}\text{Sn}$, and $n + {}^{208}\text{Pb}$ systems. The points used here can also be used for the relevant higher angular momentum t matrices.

B. Off-shell behavior of the optical potential and its separable representation

After having established the scheme for finding separable representations of the t matrices obtained from the CH89 phenomenological optical potential and checking its accuracy

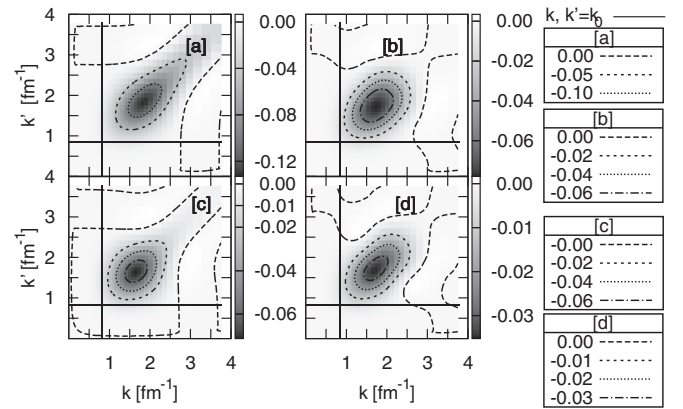


FIG. 6. The $l = 6$, $j = 13/2$ partial wave off-shell t -matrix elements, $t_6(k', k; E_{c.m.})$, for the $n + {}^{48}\text{Ca}$ system computed at $E_{c.m.} = 16$ MeV as a function of the off-shell momenta k' and k . The on-shell momentum, $k_0 = 0.87 \text{ fm}^{-1}$, is indicated by the straight lines. Panels [a] and [c] show the real and imaginary parts of the t matrix in units of fm^2 obtained from the CH89 [6] phenomenological optical potential, while panels [b] and [d] depict their separable representation (rank 3). Note the difference in scale between the left- and right-hand-side panels.

by comparing the S -matrix elements between 0 and 50 MeV, we now want to look at the resulting off-shell t matrices. The partial wave off-shell t matrices, $t_l(k', k; E)$, are calculated at a given energy E by using Eq. (14) sandwiched with arbitrary momenta k' and k .

In Fig. 6 we show the off-shell t matrix at $E_{c.m.} = 36$ MeV for the $n + {}^{48}\text{Ca}$ system in the partial wave $l = 6$, $j = 13/2$. The left-side panels ([a] and [c]) show the off-shell t matrix as a function of momenta k and k' obtained as a solution of the LS equation with the CH89 potential, while the right-hand-side panels ([b] and [d]) depict their separable representation. The on-shell momentum at $k_0 = 1.3 \text{ fm}^{-1}$ is indicated in each panel by the horizontal and vertical lines.

First, we point out that in both cases the t matrix is symmetric around the line $k' = k$, which must be the case if the underlying potential fulfills the reciprocity theorem. This also shows that our generalization of the EST scheme to complex potentials is correct. Had we used the definition given in Ref. [25], the resulting off-shell t matrix would not have this symmetry.

Second, we observe that overall the magnitude of the off-shell elements of the separable interaction is smaller than that of the t matrix of the original potential. It was shown in Ref. [26] that, for a rank-1 separable potential, the off-shell t matrix has the form $v(p)/v(k_0)$, where k_0 is the on-shell momentum, the form factors $v(p)$ are the half-shell t matrices calculated at the support points, and $v(k_0)$ is their on-shell value. This justifies why the magnitude of the off-shell elements of the separable t matrix is smaller than the magnitude of those obtained from the solution of an LS equation with the original CH89 potential.

Furthermore, we note that the t matrix obtained from the CH89 potential has significant nonvanishing values along the line $k = k'$ even for momenta $k = k' \geq 4 \text{ fm}^{-1}$, which is typical for local potentials, while these off-shell matrix

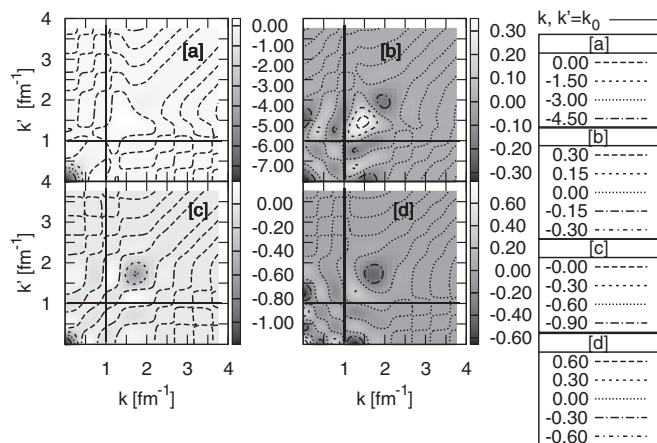


FIG. 7. The $l = 0$ partial wave off-shell t -matrix elements, $t_0(k', k; E_{c.m.})$, for the $n + {}^{208}\text{Pb}$ system computed at $E_{c.m.} = 21$ MeV as a function of the off-shell momenta k' and k . The on-shell momentum, $k_0 = 1.0$ fm $^{-1}$, is indicated by the straight lines. Panels [a] and [c] show the real and imaginary parts of the t matrix in units of fm 2 obtained from the CH89 [6] phenomenological optical potential, while panels [b] and [d] depict their separable representation (rank 3). Note the difference in scale between the left- and right-hand-side panels.

elements approach zero for the separable counterpart. The fact that the separable representation projects out high-momentum components of the original t matrix is reminiscent of renormalization group techniques [31], which in nuclear physics are typically applied to the NN force. We note that the off-shell dip around $k' = k \sim 1.5$ fm $^{-1}$ is present in both cases, indicating that closer to the on-shell point, the EST scheme preserves the off-shell structure.

In Fig. 7 we show the off-shell t matrix at $E_{c.m.} = 21$ MeV for the $n + {}^{208}\text{Pb}$ system in the partial wave $l = 0$. The left panels again depict the real and imaginary t matrix obtained as a solution of the LS equation with the CH89 potential, while the right panels give their separable representation. The on-shell momentum $k_0 = 1.0$ fm $^{-1}$ is indicated by horizontal and vertical lines. The scale of the exact solution is dominated by the strong dip close to the origin. This dip is also present in the separable representation; however, it is almost a factor of 4 smaller in case of the real part and a factor of 2 smaller for the imaginary part. The off-shell structure around $k' = k \sim 1.5$ fm $^{-1}$ is again captured well by the separable representation. The exact solution also has nonzero contributions along the line $k' = k$, while the separable representation does not; however, due to the scale this is not visible in the figure. For these heavier systems, the higher partial waves behave very similarly to the ones in the $n + {}^{48}\text{Ca}$ system. Therefore we do not show them separately.

IV. SUMMARY AND CONCLUSIONS

In this work we extended the well-known EST scheme [25] for creating separable representations of two-body transition matrix elements as well as potentials to the realm of complex potentials. Requiring that the separable transition matrix fulfill the reciprocity theorem, we identified a suitable rank-1

separable potential. In analogy to Ref. [25], we generalized this potential to arbitrary rank.

All calculations presented in this work are based on the Chapel Hill phenomenological optical potential CH89 [6]. Since the CH89 potential, as are nearly all phenomenological optical potentials, is given in coordinate space using Woods-Saxon functions, we first give a semianalytic Fourier transform of those Woods-Saxon functions in terms of a series expansion. In practice, it turns out that only two terms in the expansion are sufficient for achieving convergence. Note that our approach for deriving the momentum-space optical potential is general and can be applied to any optical potential of Woods-Saxon form. This momentum-space CH89 potential is then used in the partial wave LS integral equation to calculate half-shell t matrices. These then serve as input to the the generalized scheme for creating separable representations for complex potentials.

The systematic studies in this paper include $n + {}^{48}\text{Ca}$, $n + {}^{132}\text{Sn}$, and $n + {}^{208}\text{Pb}$. We are able to provide, for all cases, a systematic classification of support points for partial wave groups, so that the partial wave S matrices are reproduced to at least four significant figures compared to the original momentum-space solution of the LS equation. We find that the low partial waves of the $n + {}^{208}\text{Pb}$ system require a rank-5 separable potential to be well represented in the energy regime between 0 and 50 MeV center-of-mass energy. The support points obtained for this case are well suited to represent all partial waves of the $n + {}^{208}\text{Pb}$ as well as all lighter systems described by the CH89 optical potential.

We find that the rank required for achieving a good representation decreases with increasing angular momentum of the partial wave considered. We developed recommendations for both the rank and the locations of support points to be used when describing medium-mass and heavy systems generated from the CH89 potential. Our recommendations group together partial waves. We also demonstrated that it is sufficient to determine support points including only the central part of the optical potential; when the spin-orbit interaction is added and the form factors are accordingly modified, the same support points can be expected to yield a good representation.

We then investigated the off-shell behavior of the constructed separable representations and found that, overall, the high-momentum components along the $k = k'$ axis which are typical for local potentials are removed from the separable representation. Furthermore, the off-shell elements of the separable representation are smaller in magnitude but follow the functional shape of the CH89 potential. Since off-shell matrix elements are not observables, only reaction calculations can show if the differences seen in the off-shell t matrix have any consequences for, e.g., three-body observables. Future work will address this question.

ACKNOWLEDGMENTS

This work was performed in part under the auspices of the U.S. Department of Energy under Contract No. DE-FG02-93ER40756 with Ohio University and Contract No. DE-FG52-08NA28552 with Michigan State University and

under Contracts No. DE-SC0004084 and No. DE-SC0004087 (TORUS Collaboration) and by Lawrence Livermore National Laboratory under Contract No. DE-AC52-07NA27344. F. M. Nunes also acknowledges support from the National Science Foundation under Grant No. PHY-0800026. R. C. Johnson thanks the NSCL for their hospitality and support during his visits.

APPENDIX: FOURIER TRANSFORM OF GLOBAL OPTICAL POTENTIALS

1. Global optical potentials in coordinate space

Most global optical potentials are parametrized in terms of Wood-Saxon form factors and its derivatives. For convenience, here we provide the definitions of the form factor and standard parametrizations of phenomenological optical potentials. These definitions are also those for the CH89 potential [6], which we use throughout this work. The short-range, nuclear part is given by

$$U_{\text{nucl}}(r) = V(r) + i[W(r) + W_s(r)] + V_{ls}(r) \mathbf{l} \cdot \boldsymbol{\sigma}, \quad (\text{A1})$$

where

$$\begin{aligned} V(r) &= -V_r f_{ws}(r, R_0, a_0), \\ W(r) &= -W_v f_{ws}(r, R_s, a_s), \\ W_s(r) &= -W_s(-4a_s) f'_{ws}(r, R_s, a_s), \\ V_{ls}(r) &= -(V_{so} + iW_{so})(-2)g_{ws}(r, R_{so}, a_{so}), \end{aligned} \quad (\text{A2})$$

$$\begin{aligned} f_{ws}(r, R, a) &= \frac{1}{1 + \exp\left(\frac{r-R}{a}\right)}, \\ f'_{ws}(r, R, a) &= \frac{d}{dr} f_{ws}(r, R, a), \\ g_{ws}(r, R, a) &= f'_{ws}(r, R, a)/r. \end{aligned} \quad (\text{A3})$$

The constants V_r , W_v , V_{so} , and W_{so} are the strength parameters, and a and R are the diffuseness and the radius parameters given in Ref. [6].

2. Fourier transform of Woods-Saxon functions

The basic functions to be transformed to momentum space are given by Eqs. (A3), which are the Woods-Saxon function and its derivative. The Fourier transform of, e.g., $V(r)$ of Eq. (A2) is given by

$$V(q) = \frac{1}{2\pi^2} \frac{1}{q} \int_0^\infty dr r V(r) \sin(qr), \quad (\text{A4})$$

where q is the momentum transfer defined as $q = |\mathbf{q}' - \mathbf{k}|$.

Introducing dimensionless variables $\rho_k = qa_k$, $z = r/a_k$, $\alpha_k = R_k/a_k$, and $\gamma_k = e^{-\alpha_k}$ (with $k \equiv 0, s, so$) and inserting into Eq. (A4) yields

$$\begin{aligned} V(q) &= -\frac{V_r}{2\pi^2} \frac{a_0^2}{q} \int_0^\infty dz \frac{z \sin(\rho_0 z)}{1 + \exp(z - \alpha_0)} \\ &\equiv -\frac{V_r}{2\pi^2} \frac{a_0^2}{q} \Im m \int_0^\infty dz \frac{z \exp(i\rho_0 z)}{1 + \exp(z - \alpha_0)}. \end{aligned} \quad (\text{A5})$$

Repeating the above step for all the expressions in Eqs. (A2) yields expressions that are similar to Eq. (A5). There are

four distinct real integrals appearing in the Fourier transform expressions of Eqs. (A2) and they are the real and imaginary parts of the two complex integrals I_1 and I_2 such that

$$\begin{aligned} I_1(\rho_k, \alpha_k) &= \int_0^\infty dz \frac{z \exp(i\rho_k z)}{1 + \exp(z - \alpha_k)} \equiv \int_0^\infty f_1(z) dz, \\ I_2(\rho_k, \alpha_k) &= \int_0^\infty dz \frac{\exp(i\rho_k z)}{1 + \exp(z - \alpha_k)} \equiv \int_0^\infty f_2(z) dz, \end{aligned} \quad (\text{A6})$$

where ρ_k and α_k are real numbers. With the definitions given in Eq. (A6) the Fourier transforms of the expressions given in Eqs. (A2) can be written as

$$\begin{aligned} V(q) &= -\frac{V_r}{2\pi^2} \frac{a_0^2}{q} \Im m I_1(\rho_0, \alpha_0), \\ W(q) &= -\frac{W_v}{2\pi^2} \frac{a_s^2}{q} \Im m I_1(\rho_s, \alpha_s), \\ W_s(q) &= -\frac{2W_s}{\pi^2} a_s^2 \left[\frac{1}{q} \Im m I_2(\rho_s, \alpha_s) + a_s \Re e I_1(\rho_w, \alpha_s) \right], \\ V_{ls}(q) &= -\frac{(V_{so} + W_{so})}{\pi^2} a_{so} \Re e I_2(\rho_{so}, \alpha_{so}). \end{aligned} \quad (\text{A7})$$

The integrals I_1 and I_2 can be evaluated by contour integration. The closed integration loop is taken to be the boundary of the first quadrant (i.e., from 0 to ∞ along the positive real axis, then a circular path from $+\infty$ to $+i\infty$, and finally from $+i\infty$ to 0 along the positive imaginary axis). The contribution from the circular path integral is zero in this case. Both integrands have poles at $z_n = \alpha + i\pi(2n+1)$ with $n \in \mathbf{Z}$. The corresponding residues are given by

$$\begin{aligned} \text{Res}(z_n, f_1) &= -[\alpha + i\pi(2n+1)] e^{i\rho\alpha} e^{-(2n+1)\pi\rho}, \\ \text{Res}(z_n, f_2) &= -e^{i\rho\alpha} e^{-(2n+1)\pi\rho}. \end{aligned} \quad (\text{A8})$$

The total closed-loop integral is obtained via the residue theorem, and the path from $+i\infty$ to 0 is evaluated as a series expansion of the integrand in terms of γ . This leads to

$$\begin{aligned} \Re e I_1(\rho, \alpha) &= \frac{2\pi e^{-\pi\rho}}{(1 - e^{-2\pi\rho})^2} [\pi(1 + e^{-2\pi\rho}) \cos(\rho\alpha) \\ &\quad + \alpha(1 - e^{-2\pi\rho}) \sin(\rho\alpha)] \\ &\quad - \sum_{n=0}^{\infty} (-1)^n \gamma^n \frac{\rho^2 - n^2}{(\rho^2 + n^2)^2}, \\ \Im m I_1(\rho, \alpha) &= \frac{2\pi e^{-\pi\rho}}{(1 - e^{-2\pi\rho})^2} [\pi(1 + e^{-2\pi\rho}) \sin(\rho\alpha) \\ &\quad - \alpha(1 - e^{-2\pi\rho}) \cos(\rho\alpha)] \\ &\quad - 2 \sum_{n=0}^{\infty} (-1)^n \gamma^n \frac{n\rho}{(\rho^2 + n^2)^2}, \\ \Re e I_2(\rho, \alpha) &= \frac{2\pi e^{-\pi\rho}}{1 - e^{-2\pi\rho}} \sin(\rho\alpha) - \sum_{n=0}^{\infty} (-1)^n \gamma^n \frac{n}{\rho^2 + n^2}, \\ \Im m I_2(\rho, \alpha) &= -\frac{2\pi e^{-\pi\rho}}{1 - e^{-2\pi\rho}} \cos(\rho\alpha) + \sum_{n=0}^{\infty} (-1)^n \gamma^n \frac{\rho}{\rho^2 + n^2}. \end{aligned} \quad (\text{A9})$$

TABLE II. Numerical values of the sums of Eqs (A10) evaluated for $\rho = 0.5$ and $\alpha = 5.8$ (corresponding to $A = 40$): results for CH89 [6]. The series is summed up to the value of n_{\max} listed in the first column.

n_{\max}	S_1^R	S_1^I	S_2^R	S_2^I
0	-4.000 000	0.000 000	0.000 000	2.000 000
1	-4.023 898	0.031 864	0.039 830	1.980 085
2	-4.023 383	0.031 589	0.038 663	1.980 377
3	-4.023 396	0.031 594	0.038 703	1.980 370

Similar expressions were derived in Ref. [32]. The infinite sums cannot be evaluated analytically and their convergence properties need to be studied numerically. In order to do so, let us define the finite sums S_1^R , S_1^I , S_2^R , and S_2^I as

$$\begin{aligned}
S_1^R &= - \sum_{n=0}^{n_{\max}} (-1)^n \gamma^n \frac{\rho^2 - n^2}{(\rho^2 + n^2)^2}, \\
S_1^I &= -2 \sum_{n=0}^{n_{\max}} (-1)^n \gamma^n \frac{n\rho}{(\rho^2 + n^2)^2}, \\
S_2^R &= - \sum_{n=0}^{n_{\max}} (-1)^n \gamma^n \frac{n}{\rho^2 + n^2}, \\
S_2^I &= \sum_{n=0}^{n_{\max}} (-1)^n \gamma^n \frac{\rho}{\rho^2 + n^2}.
\end{aligned} \tag{A10}$$

The convergence of the above sums is studied as a function of n_{\max} . The parameter crucial to the convergence is $\gamma = e^{-\alpha}$; the smaller the value of γ , the faster the series will converge. Thus, the slowest convergence will be for the smallest values of α for a given optical potential. For the CH89 optical potential [6] the minimum value is slightly larger than 5.8, corresponding to mass number $A = 40$. For all heavier nuclei α is larger. The numerical values of the sums of Eqs. (A10) are given in Table II as function of n_{\max} for the worst case of $\alpha = 5.8$. The table demonstrates that for the CH89 global optical potential $n_{\max} = 2$ is sufficient to obtain convergence up to six decimal points.

The truncation discussed above focused on CH89. The conditions for convergence should be tested for other global optical potentials. We repeated the study for the Weppner-Penny [7] (WP) global optical potential, which was fitted to nuclei as light as ^{12}C . Then, the required minimal value of α is about 3, where we consider that α is energy dependent. In Table III, we present the convergence of the sums of Eqs. (A10) for the fixed value $\alpha = 3.0$, when using the WP potential. We find that $n_{\max} = 4$ is sufficient to obtain convergence up to six decimal points. For the heavier nuclei, $A \geq 40$, the WP optical potential requires only $n_{\max} = 2$, similar to the CH89 optical potential.

3. The partial wave optical potential in momentum space

According to the considerations in the previous section the first two terms in the series expansion are sufficient to obtain momentum-space expressions for the Fourier transforms of

TABLE III. Numerical values of the sums of Eqs (A10) evaluated for $\rho = 0.5$ and $\alpha = 3.0$ (corresponding to $A = 12$): results for WP [7]. The series is summed up to the value of n_{\max} listed in the first column.

n_{\max}	S_1^R	S_1^I	S_2^R	S_2^I
0	-4.000 000	0.000 000	0.000 000	2.000 000
1	-4.001 453	0.031 864	0.039 830	1.998 789
2	-4.001 451	0.031 589	0.038 663	1.998 790
3	-4.001 451	0.031 594	0.038 703	1.998 790
4	-4.023 395	0.031 593	0.038 702	1.980 370
5	-4.023 395	0.031 593	0.038 702	1.980 370

the Woods-Saxon functions of the CH89 potential, which are sufficiently accurate as shown in Table II. This leads to

$$\begin{aligned}
V(q) &= \frac{V_r}{\pi^2} \left\{ \frac{\pi a_0 e^{-\pi a_0 q}}{q(1 - e^{-2\pi a_0 q})^2} [R_0(1 - e^{-2\pi a_0 q}) \cos(qR_0) \right. \\
&\quad \left. - \pi a_0(1 + e^{-2\pi a_0 q}) \sin(qR_0)] \right. \\
&\quad \left. - a_0^3 e^{-\frac{R_0}{a_0}} \left[\frac{1}{(1 + a_0^2 q^2)^2} - \frac{2e^{-\frac{R_0}{a_0}}}{(4 + a_0^2 q^2)^2} \right] \right\} \tag{A11}
\end{aligned}$$

for the Fourier transform of $V(r)$. Here q stands for the magnitude of the momentum transfer as defined in the previous section.

For $W(q)$, the imaginary volume term, the same expression is obtained with W_v , a_s , and R_s in the place of V_r , a_0 , and R_0 .

For the surface term $W_s(r)$ of Eq. (A2) we obtain the following momentum-space form:

$$\begin{aligned}
W_s(q) &= -4a_s \frac{W_s}{\pi^2} \left\{ \frac{\pi a_s e^{-\pi a_s q}}{(1 - e^{-2\pi a_s q})^2} \right. \\
&\quad \times \left[\left(\pi a_s(1 + e^{-2\pi a_s q}) - \frac{1}{q}(1 - e^{-2\pi a_s q}) \right) \cos(qR_s) \right. \\
&\quad \left. \left. + R_s(1 - e^{-2\pi a_s q}) \sin(qR_s) \right] \right. \\
&\quad \left. + a^2 e^{-R_s/a_s} \left[\frac{1}{(1 + a_s^2 q^2)^2} - \frac{4e^{-R_s/a_s}}{(4 + a_s^2 q^2)^2} \right] \right\}. \tag{A12}
\end{aligned}$$

The Fourier transform of the spin-orbit term, $V_{ls}(r)$, leads to

$$\begin{aligned}
V_{ls}(q) &= -\frac{a_{so}}{\pi^2} (V_{so} + iW_{so}) \left\{ \frac{2\pi e^{-\pi a_{so} q}}{1 - e^{-2\pi a_{so} q}} \sin(qR_{so}) \right. \\
&\quad \left. + e^{-\frac{R_{so}}{a_{so}}} \left(\frac{1}{1 + a_{so}^2 q^2} - \frac{2e^{-\frac{R_{so}}{a_{so}}}}{4 + a_{so}^2 q^2} \right) \right\}. \tag{A13}
\end{aligned}$$

Here \mathbf{q} is the momentum transfer, $\mathbf{q} = \mathbf{k}' - \mathbf{k}$ with $|\mathbf{q}| = \sqrt{k'^2 + k^2 - 2k'k \cos \theta_{k'k}}$.

The most general form of a momentum-space potential is usually written as $\langle \mathbf{k}' | U_{\text{nucl}} | \mathbf{k} \rangle \equiv U_{\text{nucl}}(\mathbf{k}', \mathbf{k})$, with \mathbf{k}' and \mathbf{k} being linear independent vectors spanning the scattering plane. A local potential only depends on the momentum transfer, $\mathbf{k}' - \mathbf{k}$, and has no contribution proportional to the orthogonal vector $\frac{1}{2}(\mathbf{k}' + \mathbf{k})$. Thus, in momentum space the most general

form of an optical potential of Eq. (A1) takes the form

$$U_{\text{nuc1}}(\mathbf{k}', \mathbf{k}) = V_c(\mathbf{k}', \mathbf{k}) + i \sin \theta_{kk'} V_s(\mathbf{k}', \mathbf{k}) \sigma \cdot \hat{\mathbf{n}}, \quad (\text{A14})$$

where $\hat{\mathbf{n}}$ is the vector perpendicular to the scattering plane spanned by the vectors \mathbf{k} and \mathbf{k}' , and $V_s = \frac{d}{dx} V_{ls}$ with $x = \cos \theta_{kk'}$. $V_c(\mathbf{k}', \mathbf{k})$ is the sum of the three central interaction terms of Eq. (A14). For the partial wave decomposition one obtains (see, e.g., Ref. [33])

$$\begin{aligned} V_c(\mathbf{k}', \mathbf{k}) &= \frac{1}{4\pi} \sum_{l=0}^{\infty} [(l+1)V_{l+}(k', k) + lV_{l-}(k', k)] P_l(x), \\ V_s(\mathbf{k}', \mathbf{k}) &= \frac{d}{dx} V_{ls}(\mathbf{k}', \mathbf{k}) \\ &= \frac{1}{4\pi} \frac{d}{dx} \sum_{l=0}^{\infty} [V_{l+}(k', k) - V_{l-}(k', k)] P_l(x). \end{aligned} \quad (\text{A15})$$

Using the standard orthogonality relations for the Legendre polynomials leads to the partial wave projected potential for a spin-0 + spin-1/2 system:

$$\begin{aligned} V_{l+}(k', k) &= 2\pi \int_{-1}^1 dx P_l(x) V_c(\mathbf{k}', \mathbf{k}) \\ &\quad + 2\pi l \int_{-1}^1 dx P_l(x) V_{ls}(\mathbf{k}', \mathbf{k}), \\ V_{l-}(k', k) &= 2\pi \int_{-1}^1 dx P_l(x) V_c(\mathbf{k}', \mathbf{k}) \\ &\quad - 2\pi(l+1) \int_{-1}^1 dx P_l(x) V_{ls}(\mathbf{k}', \mathbf{k}), \end{aligned} \quad (\text{A16})$$

TABLE IV. The partial wave phase shift $\delta_{l=1, j=\frac{3}{2}}$ calculated from the CH89 [6] optical potential for $n + {}^{48}\text{Ca}$ elastic scattering as a function of the projectile laboratory energy. The second column shows phase shifts computed in momentum space, while the third column gives the coordinate-space calculation based on the coupled-channel code FRESKO [29].

E_{lab} (MeV)	$\delta_{l=1, j=\frac{3}{2}}$ (deg)	
	k space	r space
5	(-73.78, 13.75)	(-73.84, 13.75)
10	(66.24, 17.02)	(66.18, 17.00)
20	(18.09, 19.51)	(18.02, 19.45)
40	(-38.03, 22.48)	(-38.08, 22.47)
50	(-57.83, 23.48)	(-57.88, 23.47)

where the indices refer to $j = l + \frac{1}{2}$ and $j = l - \frac{1}{2}$, respectively. The partial wave projected potential matrix enters a two-body LS equation, from which the standard scattering phase shifts are obtained.

To test the quality of the momentum-space representation of the CH89 optical potential, we compare scattering phase shifts obtained in momentum space with those independently calculated in coordinate space using the techniques implemented in the coupled-channel code FRESKO [29]. This comparison is given in Table IV for $n + {}^{48}\text{Ca}$ for projectile kinetic energies up to 50 MeV. The agreement is satisfactory and gives us confidence for using the momentum-space representation of the CH89 global optical potential as a starting point for constructing separable representations thereof.

- [1] J. E. Escher, J. T. Burke, F. S. Dietrich, N. D. Scielzo, I. J. Thompson, and W. Younes, *Rev. Mod. Phys.* **84**, 353 (2012).
- [2] J. Cizewski *et al.*, *J. Phys. Conf.* **420**, 012058 (2013).
- [3] R. Kozub *et al.*, *Phys. Rev. Lett.* **109**, 172501 (2012).
- [4] K. Schmitt *et al.*, *Phys. Rev. Lett.* **108**, 192701 (2012).
- [5] K. Jones *et al.*, *Phys. Rev. C* **84**, 034601 (2011).
- [6] R. Varner, W. Thompson, T. McAbee, E. Ludwig, and T. Clegg, *Phys. Rep.* **201**, 57 (1991).
- [7] S. P. Weppner, R. B. Penney, G. W. Diffendale, and G. Vittorini, *Phys. Rev. C* **80**, 034608 (2009).
- [8] A. Koning and J. Delaroche, *Nucl. Phys. A* **713**, 231 (2003).
- [9] F. D. Becchetti, Jr. and G. W. Greenlees, *Phys. Rev.* **182**, 1190 (1969).
- [10] A. Deltuva and A. C. Fonseca, *Phys. Rev. C* **79**, 014606 (2009).
- [11] A. Deltuva, *Phys. Rev. C* **79**, 054603 (2009).
- [12] F. M. Nunes and A. Deltuva, *Phys. Rev. C* **84**, 034607 (2011).
- [13] N. J. Upadhyay, A. Deltuva, and F. M. Nunes, *Phys. Rev. C* **85**, 054621 (2012).
- [14] A. M. Mukhamedzhanov, V. Eremenko, and A. I. Sattarov, *Phys. Rev. C* **86**, 034001 (2012).
- [15] J. Haidenbauer and W. Plessas, *Phys. Rev. C* **27**, 63 (1983).
- [16] J. Haidenbauer, Y. Koike, and W. Plessas, *Phys. Rev. C* **33**, 439 (1986).
- [17] G. H. Berthold, A. Stadler, and H. Zankel, *Phys. Rev. C* **41**, 1365 (1990).
- [18] W. A. Schnizer and W. Plessas, *Phys. Rev. C* **41**, 1095 (1990).
- [19] D. R. Entem, F. Fernandez, and A. Valcarce, *J. Phys. G* **27**, 1537 (2001).
- [20] T. Ueda and Y. Ikegami, *Prog. Theor. Phys.* **91**, 85 (1994).
- [21] A. Gal and H. Garcilazo, *Nucl. Phys. A* **864**, 153 (2011).
- [22] A. Ghovanlou and D. R. Lehman, *Phys. Rev. C* **9**, 1730 (1974).
- [23] A. Eskandarian and I. R. Afnan, *Phys. Rev. C* **46**, 2344 (1992).
- [24] K. Miyagawa and Y. Koike, *Prog. Theor. Phys.* **82**, 329 (1989).
- [25] D. Ernst, C. Shakin, and R. Thaler, *Phys. Rev. C* **8**, 46 (1973).
- [26] D. Ernst, J. Londergan, E. Moniz, and R. Thaler, *Phys. Rev. C* **10**, 1708 (1974).
- [27] B. C. Pearce, *Phys. Rev. C* **36**, 471 (1987).
- [28] D. Huber, H. Witala, A. Nogga, W. Gloeckle, and H. Kamada, *Few-Body Syst.* **22**, 107 (1997).
- [29] I. J. Thompson, *Comput. Phys. Rep.* **7**, 167 (1988).
- [30] C. Lovelace, *Phys. Rev.* **135**, B1225 (1964).
- [31] S. K. Bogner, R. J. Furnstahl, and R. J. Perry, *Phys. Rev. C* **75**, 061001(R) (2007).
- [32] M. Rodriguez-Gallardo, A. Deltuva, E. Cravo, R. Crespo, and A. C. Fonseca, *Phys. Rev. C* **78**, 034602 (2008).
- [33] R. Landau, *Quantum Mechanics II: A Second Course in Quantum Theory* (Wiley-VCH, New York, 2007).